Eur. Phys. J. D (2019) 73: 4
https://doi.org/10.1140/epjd/e2018-90537-4

THE EUROPEAN PHYSICAL JOURNAL D

Regular Article

Evaluation of differential cross sections using classical two-active electron models for He*

Nicolás Bachi[a] and Sebastian Otranto

Instituto de Física del Sur (IFISUR), Departamento de Física, Universidad Nacional del Sur (UNS), CONICET, Av. L. N. Alem 1253, B8000CPB - Bahía Blanca, Argentina

Received 30 September 2018 / Received in final form 27 October 2018
Published online 10 January 2019
© EDP Sciences / Società Italiana di Fisica / Springer-Verlag GmbH Germany, part of Springer Nature, 2019

Abstract. Differential cross sections for charge-exchange and single and double electronic emission in collisions of protons with He atoms at intermediate impact energies are theoretically evaluated by means of two classical trajectory Monte Carlo methods. These models incorporate momentum-dependent terms to the Hamiltonian in order to avoid the classical autoionization of He. The theoretical results for single capture and single ionization are compared to available experimental data. The role of the electron–electron correlation effects in double ionization processes is analyzed by inspecting the angular and energetic dependence of the electronic emission spectra at different impact energies.

1 Introduction

Unlike its quantum-mechanical counterpart, the classical He atom is unstable. A short evolution in time shows one of the electrons being emitted to the continuum while the other acquires a binding energy much lower than that corresponding to the $He^+(1s)$ state. This process takes place keeping the energy of the entire system (two bound electrons plus the nucleus) constant throughout the simulation. This issue has therefore promoted the development of different alternatives to explicitly deal with the two target electrons within the classical trajectory Monte Carlo (CTMC) method. These are: (i) the Bohr atom model [1]; (ii) models that turn off the e–e interactions and consider different sort of screenings (either static or dynamic) [2–4]; (iii) the backward–forward propagation scheme [5,6], and (iv) the introduction of additional potential terms to avoid the spontaneous autoionization [7–9]. The first alternative leads to a stable system as long as it is not disturbed, whereas the models in which the $e-e$ interaction is not explicitly considered, fail to describe electronic emission mechanisms based on the $e-e$ interaction. On the other hand, the backward–forward approach has been implemented for electron collisions but its performance for highly charged particles and low impact energies remains undetermined. The methods proposed by Kirschbaum and Wilets [7] and explored by Zajfman and Mahor [8] and Cohen [9] consist in adding momentum-dependent potentials to the actual Hamiltonian of the He atom in order to prevent the autoionization. In a recent work, we have shown that these methodologies provide a suitable representation of the He atom for specific sets of parameters for the momentum-dependent potentials [10].

In this work, we extend our previous analyses and evaluate the methods introduced in references [7–9] at a differential scale. Up to our knowledge, previous works regarding ion collisions with He have been focused on the determination of total cross sections for the different reaction channels. In Section 2, we briefly present the methodology employed. In Section 3, results are shown and analyzed, focusing on the momentum distributions of the resulting fragments for the single capture and single ionization (SI) channels. The main trends of the electronic emission spectra for the double ionization (DI) process at intermediate to low impact energies are analyzed focusing on the visible fingerprints of the electron–electron interaction. Conclusions are drawn in Section 4.

2 Theory

We now provide a brief description of the Heisenberg core (HC) [7] and energy bounded (EB) [9] theoretical models used throughout this work. A detailed analysis of the physical implications of these models can be found in our previous article (see [10]). In both methods, the classical evolution of the system, conformed by the two electrons plus the nucleus, is evaluated by solving the Hamilton's

* Contribution to the Topical Issue "Many Particle Spectroscopy of Atoms, Molecules, Clusters and Surfaces", edited by Károly Tőkési, Béla Paripás, Gábor Pszota, and Andrey V. Solov'yov.

[a] e-mail: nicolas.bachi@uns.edu.ar

equations with a Hamiltonian,

$$H_{\rm c} = H_0 + \sum_{i=1,2} V_i^{\rm c}, \tag{1}$$

where $H_0 = \sum_{i=1,2} \left(p_i^2/2 - Z/r_i\right) + 1/r_{12}$ (the actual Hamiltonian for the He atom) and $V_i^{\rm c}$ is an additional potential term that avoids the autoionization of the atom with c = HC, EB. The HC model imposes a restriction to the one-electron phase space according to the Heisenberg principle. This restriction is applied by a momentum-dependent potential of the form,

$$V_i^{\rm HC} = \frac{\xi^2}{4\alpha r_i^2}\, e^{\left\{\alpha[1-(r_i p_i/\xi)^4]\right\}}, \tag{2}$$

where r_i and p_i are the position and canonical momentum of the ith electron, respectively. The parameters of the constraint potential are (α, ξ), where α represents the hardness of $V_i^{\rm HC}$ and ξ is related to the size of the core, i.e., if $r_i p_i \leq \xi$, the potential $V_i^{\rm HC}$ becomes very repulsive and the electron is not allowed to get close to the nucleus.

In contrast to the HC approach, in the EB formulation provided by Cohen, the constraints are applied to the one-electron Coulomb energy, i.e., $E_i^{\rm Coul} = p_i^2/2 - Z/r_i$, with an extra term of the form,

$$V_i^{\rm EB} = \frac{Z}{r_i}\, e^{\left[(E_0 - E_i^{\rm Coul})/\Gamma\right]}. \tag{3}$$

Here, Z is the nuclear charge and (Γ, E_0) are the parameters of the constraint potential. The parameter Γ represents the hardness of $V_i^{\rm EB}$ and E_0 represents the minimum value allowed for the one-electron energy. This additional potential term hence provides a potential barrier that does not allow one-electron energies below the selected minimum value.

We have found that different authors have based their particular choice for the parameters (α, Γ) or (ξ, E_0) on different physical limits [7,9,11,12]. Overall, these studies agree in the fact that the evaluated cross sections are much more sensitive to changes in ξ and E_0 compared to α and Γ. Different criteria to select these parameters have been previously discussed in [10]. In this work, we consider the criterion proposed by Zhou et al. [12], which can be summarized as follows: for a given numerical parameter, α or Γ depending on the case, we seek for a physical parameter (ξ or E_0) such that the minimum of the one-electron Hamiltonian,

$$H_i^{\rm c} = \frac{p_i^2}{2} - \frac{Z}{r_i} + V_i^{\rm c} \quad ({\rm c} = {\rm HC}, {\rm EB}) \tag{4}$$

matches the energy of the $He^+(1s)$ ion.

In Table 1, we show the obtained values for ξ and E_0 for fixed values of α and Γ. These particular choices lead to the correct first ionization potential. Besides, the resulting dynamics for the He atom resemble the Bohr atom, with the two electrons orbiting the nucleus at quite similar radial distances and in a collinear configuration [10].

Table 1. Parameters of the momenutm-dependent potentials.

Approach	Hardness parameter	Physical parameter
HC	$\alpha = 2.0$	$\xi = 0.894$
EB	$\Gamma = 0.3$ a.u.	$E_0 = -2.91$ a.u.

The numerical integration of the Hamilton equations for the collision system consisting in the He atom plus the projectile is performed by means of a Runge–Kutta–Gill algorithm with adaptive step size. In the final stage, the energies of the electrons with respect to the target and the projectile allow distinguishing among the different reaction channels. In particular, in this work we focus on the processes of single capture (SC), SI and DI.

3 Results

3.1 Single electron capture and single ionization

In Figure 1, we show the target recoil-ion transverse momentum (p_t) distribution for the single electron capture channel (SC) in 50, 80 and 100 keV H^+–He collisions. Present results are compared to the experimental data provided by Martin et al. [13] and the experimental and theoretical CTMC data from Focke et al. [14]. The CTMC results presented in this recent work are based on one-active electron treatment in an independent events approximation for the reaction probabilities (IEV). To help identify major differences in shape, both HC and EB-CTMC results have been multiplied by a factor (stated in the caption) in order to normalize the structures at their peak values. In concordance with CTMC-IEV, better agreement between the theoretical calculations and the experimental data is achieved for increasing impact energies. Recent CTMC studies performed within the independent electron model have led to similar physical trends that those here obtained [15]. Present EB-CTMC results are in very good agreement with those provided by CTMC-IEV. In contrast, CTMC-HC simulations lead to wider distributions that are shifted towards larger p_t-values with respect to the experimental data in the energy range explored. Total SC cross sections at the different impact energies considered are shown in Table 2.

Now turning to the SI process for $H^+ + He$ collisions, in Figure 2, we show the p_t momentum distributions of the recoil-ion, the projectile and the emitted electron for the HC- and EB-CTMC models. In both simulations, the transverse momentum distributions of the recoil-ion and the projectile are almost identical, whereas the distributions for the emitted electrons are rather narrow in comparison. This indicates that the momentum exchange occurs predominantly between the projectile and the recoil-ion in the energy range explored.

In Figure 3, we present the longitudinal momentum (p_z) distribution for the recoil-ion and the emitted electron. For the recoil-ion we observe a sharp rise at $p_{\rm rec}^{\rm min} = -v_p/2 - E_{\rm bind}/v_p$ which is associated with the electron capture to the continuum process (ECC) and indicates

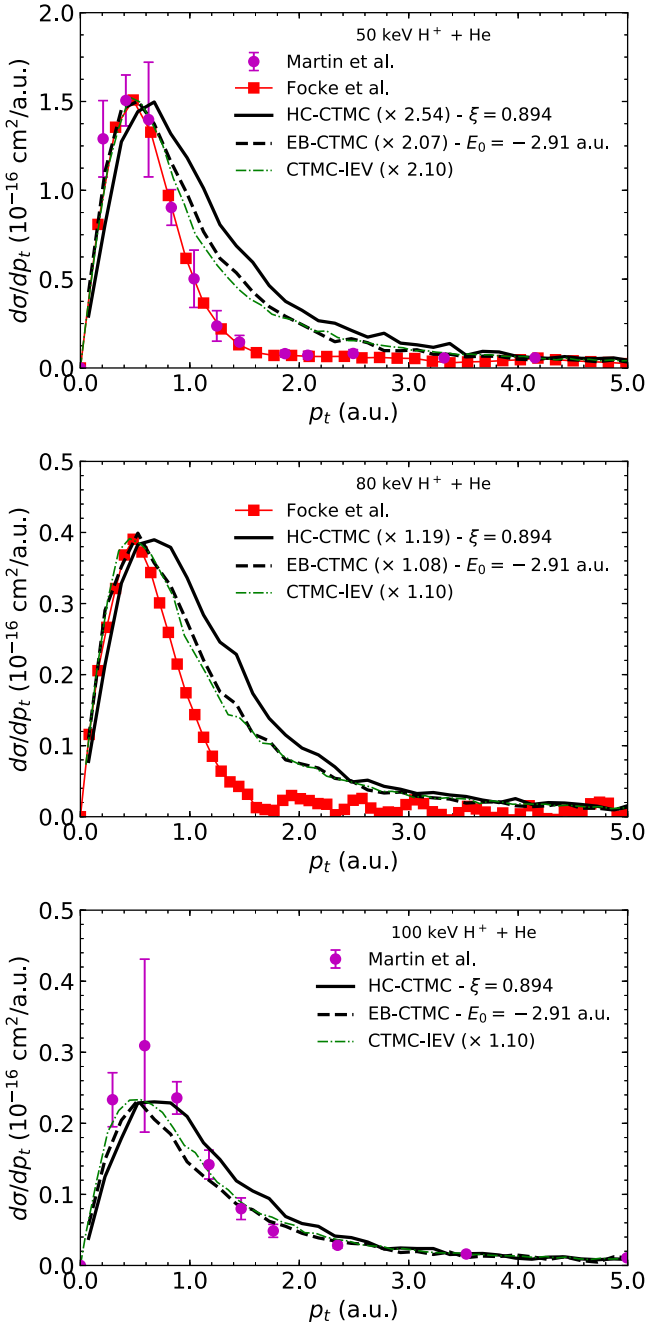

Fig. 1. Recoil-ion transverse momentum distributions in single capture processes for 50–80–100 keV H^+ + He collisions.

the minimum p_z-value attainable by the recoil-ion in an SI process. This structure moves towards the negative p_z-direction for increasing impact energies. The experimental data of Weber et al. [16] corresponding to an impact energy of 100 keV has been included and normalized to our present theoretical results. This comparison reflects the fact that the SI total cross section is underestimated by the present models (see Tab. 3), most probably due to the short radial distribution of the target electrons typical of classical treatments. Nevertheless, shape comparison indicates good agreement between the obtained

Table 2. Total cross sections (in units of 10^{-16} cm^2) for single capture (SC) channel in H^+ + He collisions.

Energy (keV)	Expt. [17,18]	HC-CTMC	EB-CTMC
50	1.01 ± 0.05^a	0.923 ± 0.007	0.994 ± 0.007
80	0.465 ± 0.023	0.549 ± 0.006	0.538 ± 0.005
100	0.272 ± 0.010	0.391 ± 0.005	0.344 ± 0.004

[a]Data at an impact energy of 48 keV.

Table 3. Total cross sections (in units of 10^{-16} cm^2) for single ionization (SI) channel in H^+ + He collisions.

Energy (keV)	Expt. [17,18]	HC-CTMC	EB-CTMC
50	0.643 ± 0.018^a	0.247 ± 0.004	0.290 ± 0.004
80	0.832 ± 0.013	0.378 ± 0.005	0.461 ± 0.005
100	0.843 ± 0.018	0.426 ± 0.005	0.514 ± 0.005

[a]Data at an impact energy of 48 keV.

structures and the data. Regarding the (p_z) distribution for the emitted electron, it can be seen that it peaks at $v_p/2$ highlighting the role of the two-center effect in the electron emission process. The experimental data of Kravis et al. [19] corresponding to an impact energy of 73 keV has been included for comparison, again normalized to our theoretical peak value, and is found in very good shape agreement with our 80 keV theoretical data.

3.2 Double ionization

In this section, we focus on differential descriptions for the DI process. Up to our knowledge, experimental differential studies for DI are scarce and restricted to much larger impact energies [20]. In this study, we have focused on the intermediate energy range and selected punctual impact energies of 100 keV and 300 keV. Total DI cross sections at these impact energies are shown in Table 4. We expect this energetic region to be rich in terms of the physical mechanisms leading to the four-body continuum. Results for the EB-CTMC model are shown only, since HC-CTMC results exhibit the same trends and are almost indistinguishable in the chosen representations. In Figures 4a and 4b, we present events histograms for the emission angle θ_1 of the first electron as a function of the emission angle θ_2 of the second electron, both angles measured from the beam direction. The obtained cross sections exhibit a symmetric structure with respect to the $\theta_2 = \theta_1$ line. Additionally, they exhibit a peak that moves towards to the rising θ_i-values as impact energy increases. At 100 eV, we observe that this maximum is located around 30° and as the impact energy increases to 300 keV moves towards 45°. It is interesting to notice the fact that at 100 keV there is a noticeable fraction of events indicating the emission of both electrons in the forward direction, feature that seems to vanish as the projectile impact energy increases.

In Figures 4c and 4d, we show the dependence of the interelectronic angle θ_{12} in terms of θ_1. As a general trend, the interelectronic angle is greater than the angles of the

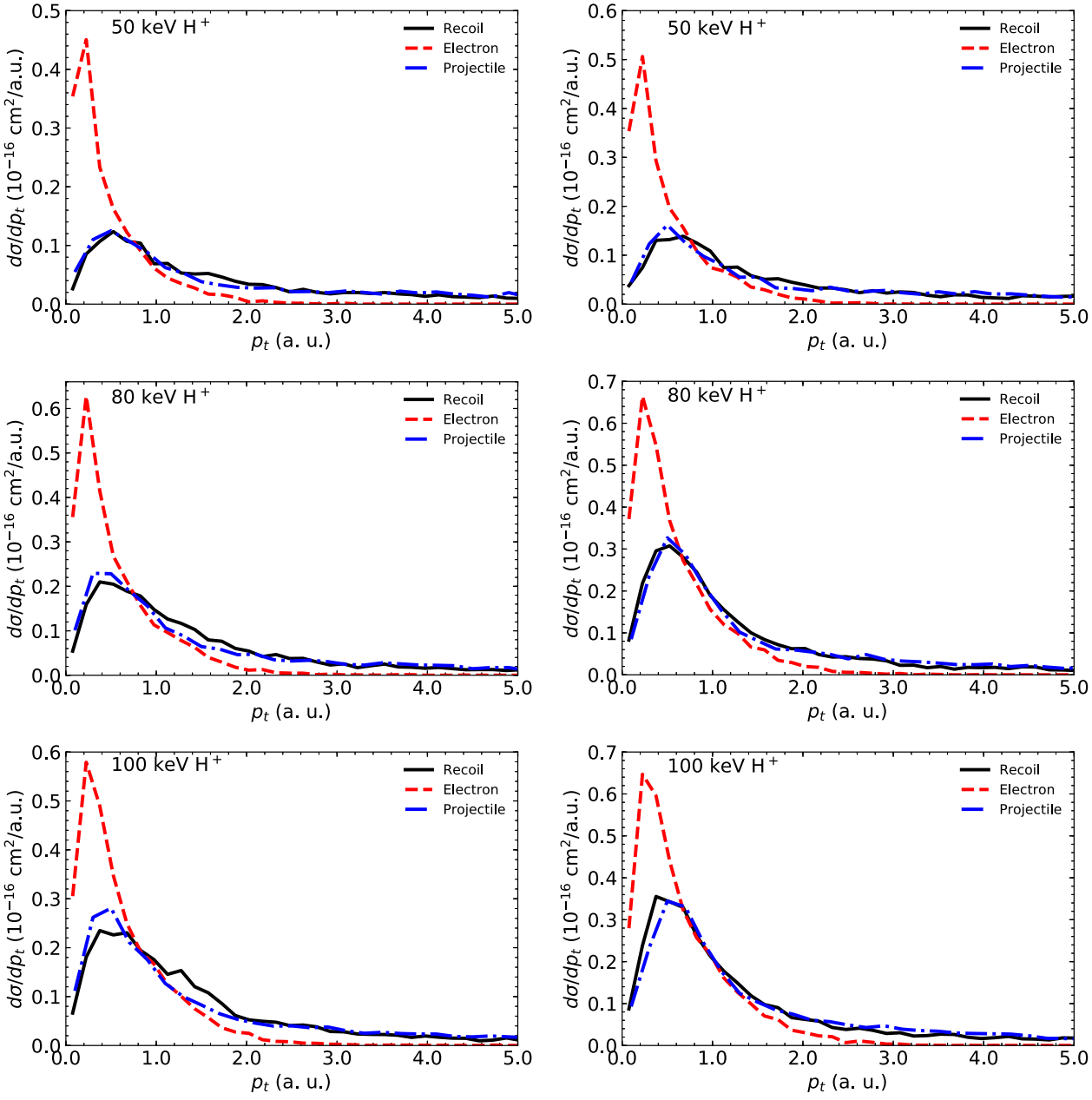

Fig. 2. Differential cross sections as a function of the transverse momentum (p_t) calculated with HC (left column) and EB-CTMC (right column) schemes in single ionization processes with 50, 80 and 100 keV impact energies.

electrons with respect to the beam direction. A geometrical inspection of these angular configurations suggests that at the impact energies explored both electrons leave the reaction region preferably in angular configurations in which the projectile is located among them. As the impact energy increases the postcollisional screening of the projectile turns less important in the electrons dynamic and electron–electron final state correlation effects are expected to become more relevant, naturally leading to larger θ_{12} angles.

In Figures 5a and 5b, we show the energy distribution for the emitted electrons. It can be seen that most of the electrons are emitted in a nearly symmetric configuration and with emission energies lower than 30 eV. The DI events distribution in terms of their relative energy and interelectronic angle are shown in Figures 5c and 5d. At 100 keV, present results suggest that both electrons are emitted in almost symmetric configurations with relative angles close to 90°. The absence of counts at low θ_{12} angles, that is clearly expected in the equal energy regime, is nicely reproduced. At an impact energy of 300 keV, we observe that the θ_{12}-value in which most of the counts are found has shifted towards 120°. This trend suggests, in concordance with our previous statements,

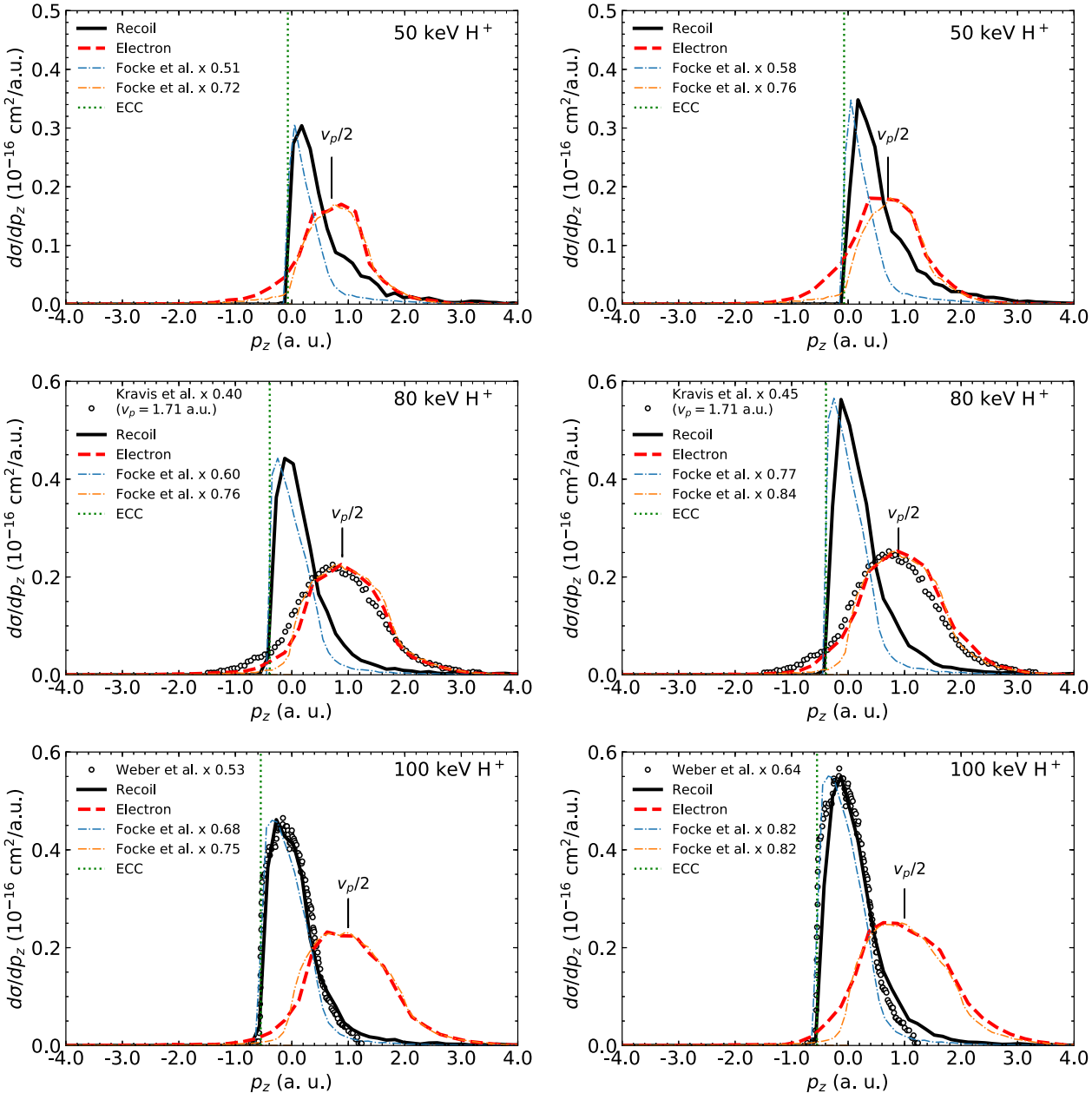

Fig. 3. Differential cross sections as a function of the longitudinal momentum (p_z) calculated with HC (left column) and EB-CTMC (right column) schemes in single ionization processes with 50, 80 and 100 keV impact energies.

that the electron–electron interaction gains relevance against the projectile postcollisional interaction as the impact energy increases.

4 Conclusions

Classical models for the He atom which incorporate momentum-dependent terms in their Hamiltonians to provide stability to the two-electron system have been evaluated at the differential scale in proton-He collisions. Present results for the recoil-ion p_t distributions for single electron capture suggest that the EB-CTMC model provides a better description of the available experimental data compared to the HC-CTMC model. For SI, both models provide similar results which are found in very good shape agreement with the available experimental data. Total cross sections magnitudes are underestimated though, possibly due to the classical finite radius for the

Table 4. Total cross sections (in units of 10^{-19} cm^2) for double ionization (DI) channel in $H^+ + He$ collisions.

Energy (keV)	Expt. [17]	HC-CTMC	EB-CTMC
100	9.61 ± 1.03	7.74 ± 0.08	8.82 ± 0.09
300	3.15 ± 0.22^a	6.81 ± 0.06	5.09 ± 0.07

[a] Data at an impact energy of 320 keV.

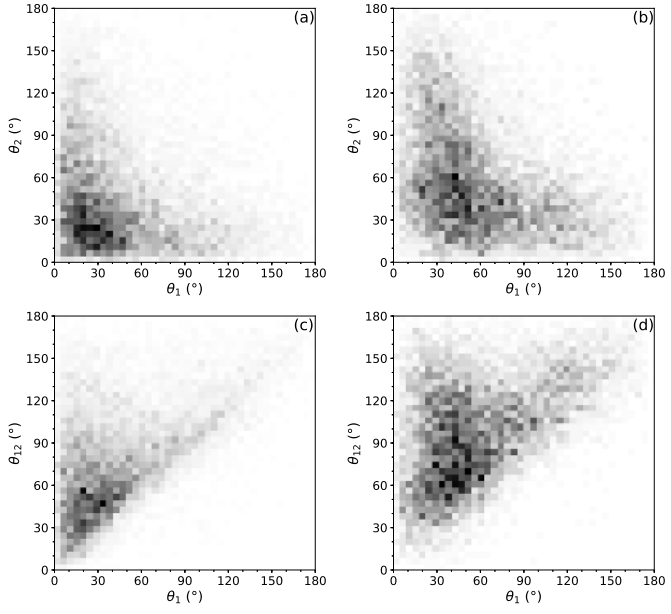

Fig. 4. Double differential cross sections for double ionization processes predicted by EB-CTMC scheme for 100 keV (left column) and 300 keV (right column) proton + He collisions (a,b) as a function of the emission angles of the electrons (θ_1, θ_2); and (c,d) as a function of as a function of the interelectronic angle (θ_{12}).

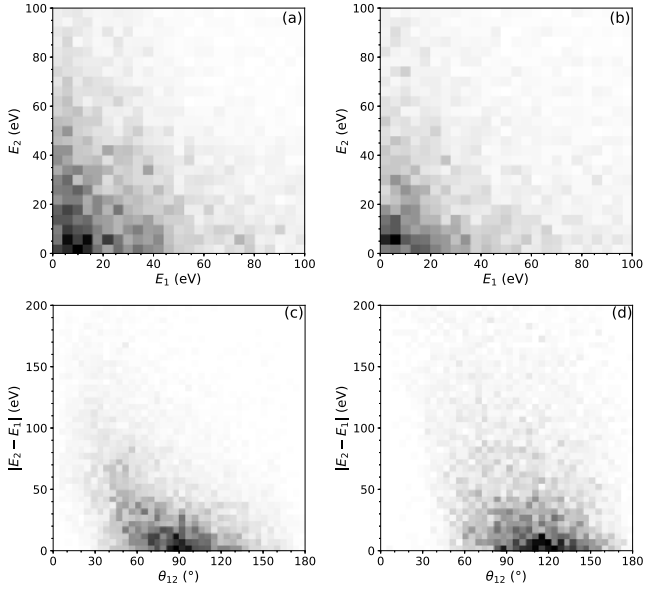

Fig. 5. Double differential cross sections for double ionization processes predicted by EB-CTMC scheme for 100 keV (left column) and 300 keV (right column) proton + He collisions (a,b) as a function of the energies of the emitted electrons (E_1, E_2); and (c,d) as a function of the relative energy and interelectronic angle $(|E_2 - E_1|, \theta_{12})$.

He atom. Present differential studies for the DI process suggest that at intermediate energies the changing role of the projectile leaves clear fingerprints in the emission geometries that evidence the four-body nature of the final state. Further experimental work regarding differential studies for the DI process would be welcome at this point.

This work has been supported by PGI 24/F073, Secretaría General de Ciencia y Tecnología, Universidad Nacional del Sur (Argentina).

Author contribution statement

All the authors were involved in the preparation of the manuscript. All the authors have read and approved the final manuscript.

References

1. M.L. McKenzie, R.E. Olson, Phys. Rev. A **35**, 2863 (1987)
2. J.S. Cohen, Phys. Rev. A **36**, 2024 (1987)
3. A.E. Wetmore, R.E. Olson, Phys. Rev. A **38**, 5563 (1988)
4. V.J. Montemayor, G. Schiwietz, Phys. Rev. A **40**, 6223 (1989)
5. T. Geyer, J.M. Rost, J. Phys. B: At. Mol. Opt. Phys. **36**, L107 (2003)
6. T. Geyer, J. Phys. B: At. Mol. Opt. Phys. **37**, 1215 (2004)
7. C.L. Kirschbaum, L. Wilets, Phys. Rev. A **21**, 834 (1980)
8. D. Zajfman, D. Maor, Phys. Rev. Lett. **56**, 320 (1986)
9. J.S. Cohen, Phys. Rev. A **54**, 573 (1996)
10. N. Bachi, S. Otranto, Eur. Phys. J. D **72**, 127 (2018)
11. S. Morita, N. Matsuda, N. Toshima, K. Hino, Phys. Rev. A **66**, 042719 (2002)
12. Y. Zhou, C. Huang, Q. Liao, P. Lu, Phys. Rev. Lett. **109**, 053004 (2012)
13. P.J. Martin, K. Arnett, D.M. Blankenship, T.J. Kvale, J.L. Peacher, E. Redd, V.C. Sutcliffe, J.T. Park, C.D. Lin, J.H. McGuire, Phys. Rev. A **23**, 2858 (1981)
14. P. Focke, R.E. Olson, N.D. Cariatore, M. Alessi, S. Otranto, Phys. Rev. A **95**, 052707 (2017)
15. A. Velayati, E. Bhanbari-Adivi, Eur. Phys. J. D **72**, 100 (2018)
16. Th. Weber, Kh. Kayyat, R. Dörner, V.D. Rodríguez, V. Mergel, O. Jagutzki, L. Schmidt, K.A. Müller, F. Afaneh, A. Gonzalez, H. Schmidt-Böcking, Phys. Rev. Lett. **86**, 224 (2001)
17. M.B. Shah, H.B. Gilbody, J. Phys. B: At. Mol. Opt. Phys. **18**, 899 (1985)
18. M.B. Shah, P. McCallion, H.B. Gilbody, J. Phys. B: At. Mol. Opt. Phys. **22**, 3037 (1989)
19. S.D. Kravis, M. Abdallah, C.L. Cocke, C.D. Lin, M. Stockli, B. Walch, Y.D. Wang, R.E. Olson, V.D. Rodríguez, W. Wu, M. Pieksma, N. Watanabe, Phys. Rev. A **54**, 1394 (1996)
20. D. Fischer, R. Moshammer, A. Dorn, J.R. Crespo López-Urrutia, B. Feuerstein, C. Höhr, C.D. Schröter, S. Hagmann, H. Kollmus, R. Mann, B. Bapat, J. Ullrich, Phys. Rev. Lett. **90**, 243201 (2003)